

Supporting Information

Boosting water evaporation via continuous formation of a 3D thin film through triple-level super-wicking routes

Guochen Jiang, Lizhong Wang, Ze Tian, Changhao Chen, Xinyu Hu, Rui Peng, Daizhou Li, Hongjun Zhang, Peixun Fan, and Minlin Zhong**

Laser Materials Processing Research Center, School of Materials Science and Engineering, Tsinghua University, Key Laboratory for Advanced Materials Processing Technology, Ministry of Education, Beijing 100084, PR China.

E-mails: zhml@tsinghua.edu.cn, fanpeixun@tsinghua.edu.cn

Supplementary Notes

Supplementary Note S1: The theoretical heat transfer coefficient of thin film evaporation on micro/nanostructured surface

The theoretical evaporation heat flux at the liquid–vapor interface is calculated by the Schrage’s derivation^{1,2}

$$\dot{q}'' = \left(\frac{2\sigma h_{fg}}{2 - \sigma}\right) \left(\frac{M}{2\pi R}\right)^{1/2} \left(\frac{P_{equ}(T_{lv})}{T_{lv}^{1/2}} - \frac{p_v(T_v)}{T_v^{1/2}}\right) \quad (S1)$$

where \dot{q}'' is the theoretical evaporation heat transfer flux at the liquid–vapor interface, σ is the evaporation adjustment coefficient related to the liquid property, h_{fg} is the enthalpy of the liquid, M is the relative molecular mass of the liquid, R is the general gas constant, P_{equ} is the equilibrium pressure, T_{lv} is the interfacial temperature at the liquid-vapor interface, p_v is the vapor pressures calculated by the Krabelon-Clausius equation (Equation S2), and T_v is the vapor temperature measured by experiment.

$$\ln\left(\frac{P_{sat}(T_{lv})}{P_v(T_v)}\right) = \frac{Mh_{fg}}{R} \left(\frac{1}{T_v} - \frac{1}{T_{lv}}\right) \quad (S2)$$

where P_{sat} is the saturation pressure at T_{lv} obtained by the handbook.

For thin film evaporation on micro/nanostructured surface, there exists deviation of P_{equ} from P_{sat} due to the effects of the disjoining pressure, Π , and capillary pressure, P_C , which can be given by

$$\ln\left(\frac{P_{equ}(T_{lv})}{P_{sat}(T_{lv})}\right) = \frac{M}{\rho_l R T_{lv}} (P_C + \Pi) \quad (S3)$$

where ρ_l is the liquid density. Considering the exist of the Kapitza resistance at the solid-liquid interface, the heat conduction in the thin film satisfied

$$T_s - T_{lv} = \left(\frac{\delta^*}{k_l} + R_k \right) q'' \quad (S4)$$

where T_s is the measured solid surface temperature, δ^* is the modified local film thickness, calculated by the ratio of thin film thickness $\delta(x)$ to surface roughness r ($\delta^*(x) = \delta(x)/r$), k_l is the liquid conductivity, and R_k is the Kapitza resistance.

Assuming $|P_{equ}(T_{lv}) - P_v(T_v)| \ll P_v(T_v)$, $|T_{lv} - T_v| \ll T_v$, and combine Equation S1~S4 with the ideal gas law, we can get

$$q'' = \frac{\left(\frac{2\sigma h_{fg}}{2-\sigma} \right) \left(\frac{M}{2\pi RT_v} \right)^{1/2} \left(\frac{P_v}{\rho_l} \right) \left[\frac{\rho_l h_{fg}}{T_v} (T_s - T_v) - (P_c + \Pi) \right]}{1 + \left(\frac{2\sigma h_{fg}}{2-\sigma} \right) \left(\frac{M}{2\pi RT_v} \right)^{1/2} \left(\frac{\rho_v h_{fg}}{T_v} \right) \left(\frac{\delta^*}{k_l} + R_k \right)} \quad (S5)$$

Thus, for thin film evaporation on micro/nanostructure surface, the heat transfer coefficient, $h = q'' / (T_s - T_v)$, is given by

$$h = \frac{\left(\frac{2\sigma h_{fg}}{2-\sigma} \right) \left(\frac{M}{2\pi RT_v} \right)^{1/2} \left(\frac{P_v}{\rho_l} \right) \left[-\frac{P_c + \Pi}{T_s - T_v} + \frac{\rho_l h_{fg}}{T_v} \right]}{1 + \left(\frac{2\sigma h_{fg}}{2-\sigma} \right) \left(\frac{M}{2\pi RT_v} \right)^{1/2} \left(\frac{\rho_v h_{fg}}{T_v} \right) \left(\frac{\delta^*}{k_l} + R_k \right)} \quad (S6)$$

Specially, we assume the temperatures of solid surface T_s and vapor T_v to be constant. For liquid film thickness much smaller than the micro/nanostructure depth, the disjoining pressure can be simplified as

$$\Pi = \frac{Ar^3}{6\pi\delta_0^3} \quad (S7)$$

where A is the Hamaker constant⁴, r is the surface roughness ratio, and δ_0 is the mean thickness of liquid thin film.

The capillary pressure $P_c(x)$ at each point on the meniscus satisfies

$$P_c(x) = \frac{\gamma \xi_L''(x)}{\sqrt{1 + [\xi_L'(x)]^2}} \quad (\text{S8})$$

where γ is the surface tension of the liquid, and $\xi_L(x)$ is the liquid thickness at each point on the meniscus.

Since all the micro/nano structures in this work are symmetrical and periodic, the capillary pressure cancels out and the averaged heat transfer coefficient of thin film evaporation in a period is given by

$$\bar{h} = \frac{\left(\frac{2\sigma h_{fg}}{2-\sigma}\right) \left(\frac{M}{2\pi RT_v}\right)^{1/2} \left(\frac{P_v}{\rho_l}\right) \left[-\frac{Ar^3}{6\pi\delta_0^3(T_s - T_v)} + \frac{\rho_l h_{fg}}{T_v}\right]}{1 + \left(\frac{2\sigma h_{fg}}{2-\sigma}\right) \left(\frac{M}{2\pi RT_v}\right)^{1/2} \left(\frac{\rho_v h_{fg}}{T_v}\right) \left(\frac{\delta_0}{rk_l} + R_k\right)} \quad (\text{S9})$$

According to the research of Sun et al^{1, 4}, there exists a linear relation between the interfacial thermal conductance (i.e., R_K^{-1}) and the surface roughness ratio, following $R_K^{-1} \propto r$.

Using Equation S9 can solve the averaged heat transfer coefficient of thin film evaporation on micro/nano structured surface with various surface roughness ratios.

Supplementary Note S2: The calculation for solar-vapor conversion efficiency

The solar-vapor conversion efficiency η , can be calculated using

$$\eta = \frac{\dot{m} h_{fg}}{A q_{solar}} \quad (S10)$$

where \dot{m} is the solar evaporation rate determined by carefully excluding dark evaporation rate \dot{m}_{dark} from the total rate of mass loss rate \dot{m}_{tot} , h_{fg} is the vaporization enthalpy on the surface, q_{solar} is the incident solar flux, and A is the solar absorbing area.

To estimate the vaporization enthalpy on the evaporator surface, the evaporation process in dark was utilized². Firstly, the evaporation rate on the surface of the TWES and pure water with the same area were measured in dark ambient environment (24 °C, RH 27%). Based on the following assumption: the energy input of bulk water and the evaporators was same, the vaporization enthalpy on the TWES could be estimated via

$$\dot{m}_{water, 24^\circ C} h_{fg, water, 24^\circ C} = \dot{m}_{TWES, 24^\circ C} h_{fg, TWES, 24^\circ C} \quad (S11)$$

where $\dot{m}_{water, 24^\circ C}$ and $\dot{m}_{TWES, 24^\circ C}$ were the measured evaporation rate of pure water and the TWES in dark, $h_{fg, water, 24^\circ C}$ and $h_{fg, TWES, 24^\circ C}$ were the vaporization enthalpy of pure water and the TWES at 24 °C, respectively. Similarly, the vaporization enthalpy of the TWES under different temperature could be estimated by

$$\dot{m}_{water, 24^\circ C} h_{fg, water, T} = \dot{m}_{TWES, 24^\circ C} h_{fg, TWES, T} \quad (S12)$$

where $h_{fg, water, T}$ and $h_{fg, TWES, T}$ were the vaporization enthalpy of pure water and the TWES at temperature T , respectively.

The vaporization enthalpy of pure water under temperature T could be calculated by

$$h_{fg, \text{ water}, T} = \int_T^{100^\circ\text{C}} C_{p,l} dT + h_{fg, \text{ water}, 100^\circ\text{C}} + \int_{100^\circ\text{C}}^T C_{p,g} dT \quad (\text{S13})$$

where $h_{fg, \text{ water}, T}$ was the vaporization enthalpy of pure water at the temperature T , $C_{p,l}$ was the heat capacity of the liquid water; $h_{fg, \text{ water}, 100^\circ\text{C}}$ was the vaporization enthalpy of the water at 100°C ($2.257 \text{ MJ}\cdot\text{kg}^{-1}$); $C_{p,g}$ was the heat capacity of the gas water, calculated by the Equation: $C_{p,g} = (3.470 + 1.45 \times 10^{-3} \times T + 0.121 \times 10^{-5} \times T^2)RM^{-1}$, R was the general gas constant, and M was the relative molecular mass of water⁵.

Based on Equation S12 and S13, the calculated parameters and results were shown below:

Evaporators	$T(\text{K})$	$h_{fg, \text{ water}, T} (\text{MJ}\cdot\text{kg}^{-1})$	$h_{fg, \text{ TWES}, T} (\text{MJ}\cdot\text{kg}^{-1})$
Mono-facial TWES-1 Sun	317.7	2.3887	0.9931
Bi-facial TWES-1 Sun	308.9	2.4098	1.0019
Bi-facial TWES-2 Sun	316.2	2.3923	0.9946
Bi-facial TWES-3 Sun	322.2	2.3804	0.9887
Bi-facial TWES-4 Sun	326.2	2.3708	0.9847

Supplementary Note S3: The analysis of heat loss

The absorbed solar energy by the evaporator Q_{solar} , can be calculated using

$$Q_{solar} = A_{solar}q_{solar} \quad (S14)$$

where A_{solar} is the area of the evaporator absorber (2×2.6 cm), and q_{solar} is the energy of the incident light ($1 \text{ kW} \cdot \text{m}^{-2}$).

Generally, the heat loss of water evaporation process has three parts, including radiation, convection and conduction^{2, 6, 7}. The calculation detail of heat loss is shown as follows:

(1) Radiation

The radiation loss was calculated by the Stefan-Boltzmann equation:

$$Q_{rad} = A\varepsilon\sigma(T_1^4 - T_0^4) \quad (S15)$$

where Q_{rad} represents the radiation loss, A is the effective area of the evaporator surface (for both face of the TWES, the area was $2 \times 2.6 \text{ cm} \times 2$), ε is the emissivity (here about 0.86), σ is the Stefan-Boltzmann constant (the value is $5.67 \times 10^{-8} \text{ W} \cdot \text{m}^{-2} \cdot \text{K}^{-4}$), T_1 is the steady-state surface temperature of the evaporator (K), and T_0 is the ambient temperature (K).

(2) Convection

The convection loss was calculated using Newton' law of cooling

$$Q_{conv} = Ah(T_1 - T_0) \quad (S16)$$

where Q_{conv} represents the convection loss, and h is the convective heat transfer

coefficient ($5 \text{ W}\cdot\text{m}^{-2}\cdot\text{K}^{-1}$).

(3) Conduction

The conduction loss was calculated using

$$Q_{cond} = Cm\Delta T \quad (\text{S17})$$

where Q_{cond} represents the conduction loss, C represents the specific heat capacity of water ($4.2 \text{ kJ}\cdot\text{K}^{-1}\cdot\text{kg}^{-1}$), m is the mass of water in the bottom tank (40 g in this work), and ΔT is the temperature change of water in the bottom tank (K) within a certain irradiation time.

The temperature parameters we used and the heat loss calculated were as follows:

Sample	T_1 (K) (two face)	T_0 (K)	ΔT (K)	$\frac{Q_{rad}}{Q_{solar}}$	$\frac{Q_{conv}}{Q_{solar}}$	$\frac{Q_{cond}}{Q_{solar}}$	Total heat loss
Mono-facial TWES	317.5, 318.1	297	0.8	23.6%	20.8%	7.2%	51.6%
Bi-facial TWES	308.7, 307.6	297	0.4	12.1%	11.1%	3.6%	26.8%

The calculated heat loss of our setup under one Sun irradiation was about 51.6% and 26.8% for mono-facial TWES and bi-facial TWES, respectively, which was agreed well with the calculated solar-vapor conversion efficiency. Notably, the bi-facial configuration could significantly reduce the heat loss, and there exists huge room for future improvement of heat utilization with the extensive exploration of highly efficient energy management in solar evaporation systems⁸.

Supporting Figure and Table

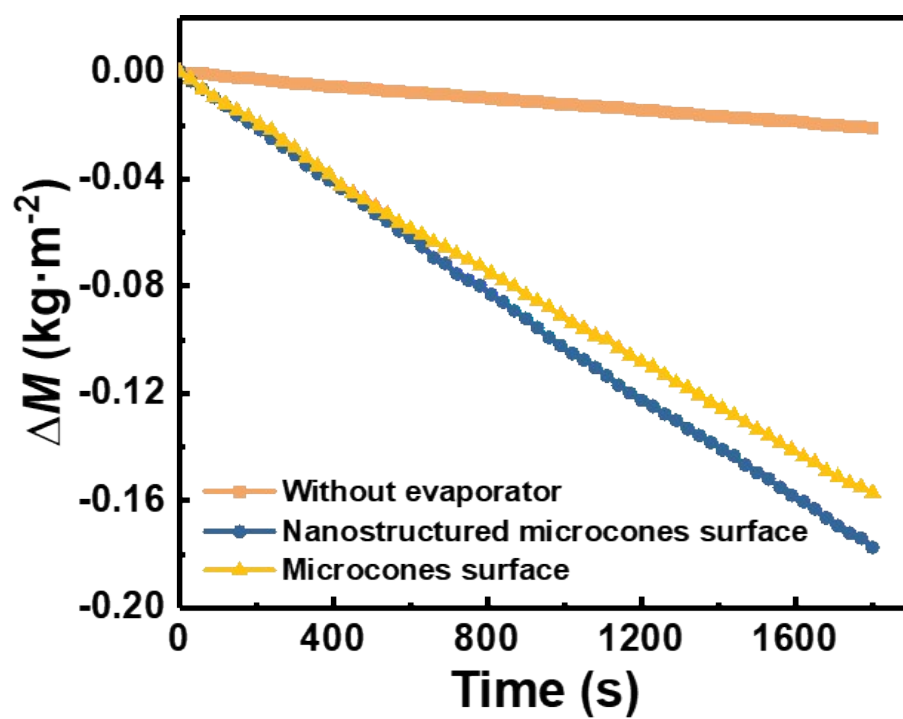


Figure S1. The water mass changes over time of the pristine copper, nanostructured microcones surface, and microcones surface in dark ambients.

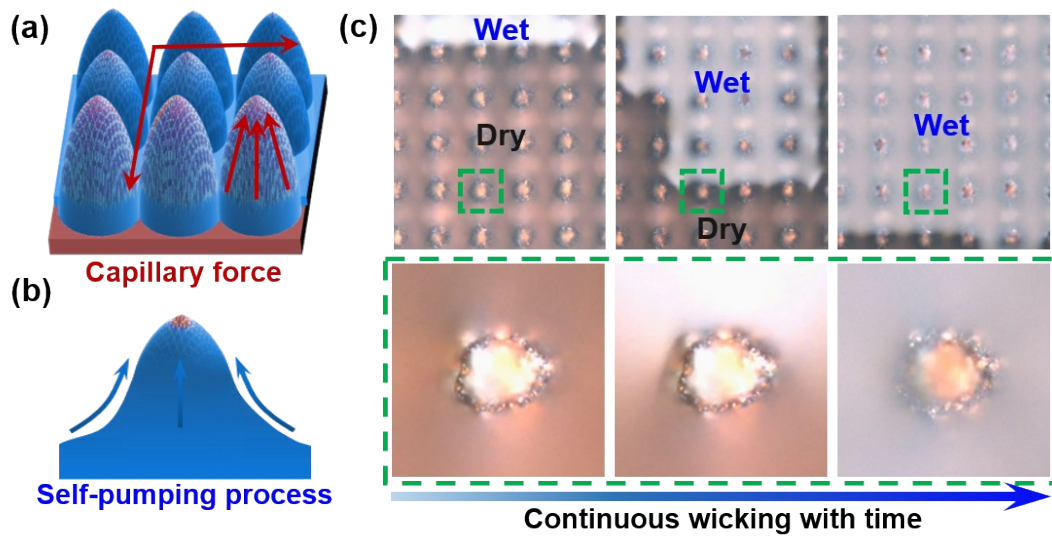


Figure S2. The wicking process on micro-nano cones surface. (a) Schematic diagram of the micro-nano cones array. Red arrows show the wicking direction of liquid under capillary force; (b) Schematic diagram of the self-pumping thin film in a single cone. Blue arrows show the self-pumping liquid; (c) The continuous wicking process of glycerol in micro-nano cones surface and a single cone.

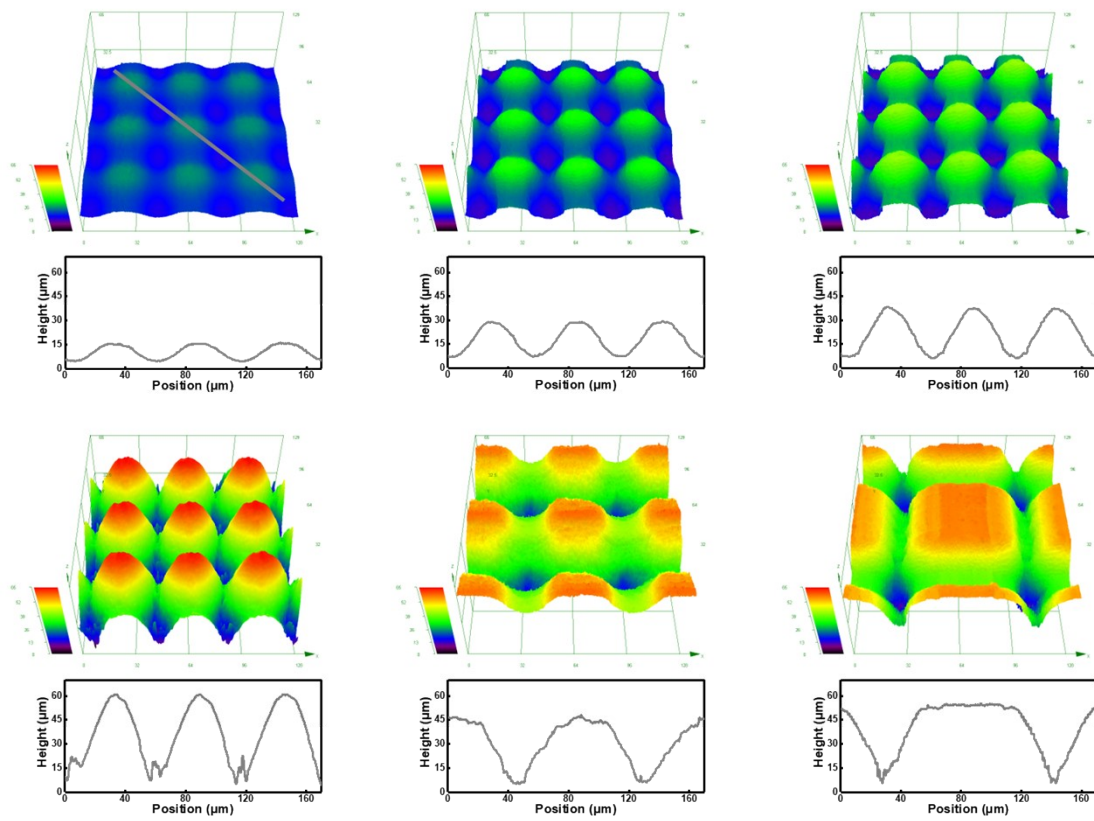


Figure S3. Micro-nano cones with various depths and diameters, and their corresponding profiles.

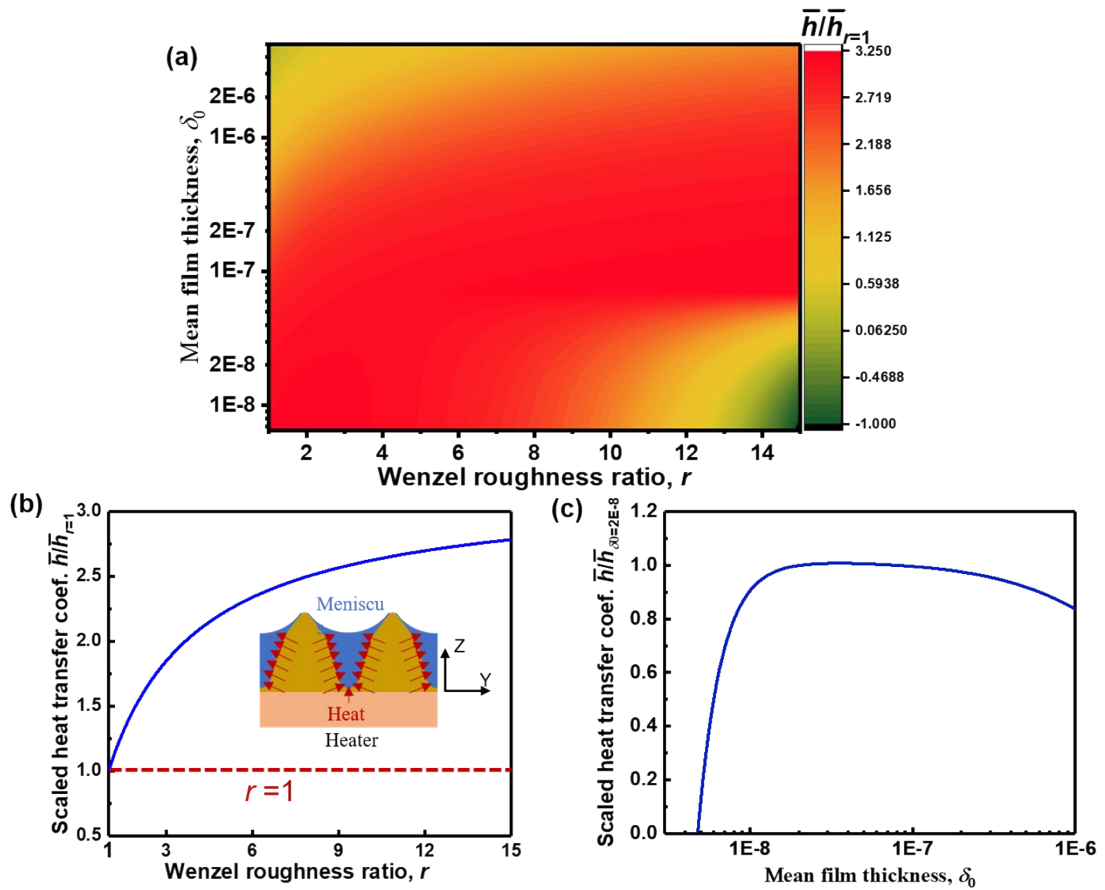


Figure S4. (a) The relationship of scaled heat transfer coefficient to the mean film thickness and Wenzel roughness ratio; (b) Scaled heat transfer coefficient of an evaporating film as a function of Wenzel roughness ratio when the mean film thickness is $6 \mu\text{m}$. Insert is the schematic diagram of the evaporation film; (c) Scaled heat transfer coefficient of an evaporating film as a function of the mean film thickness when the Wenzel roughness is 10.

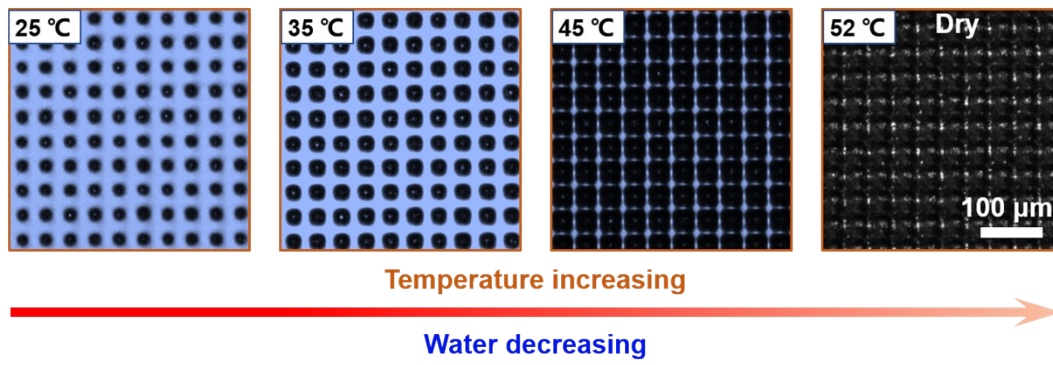


Figure S5. The water film states of the horizontal micro-nano cones surface with increasing temperature. When the temperature was 52 °C, the surface was dry.

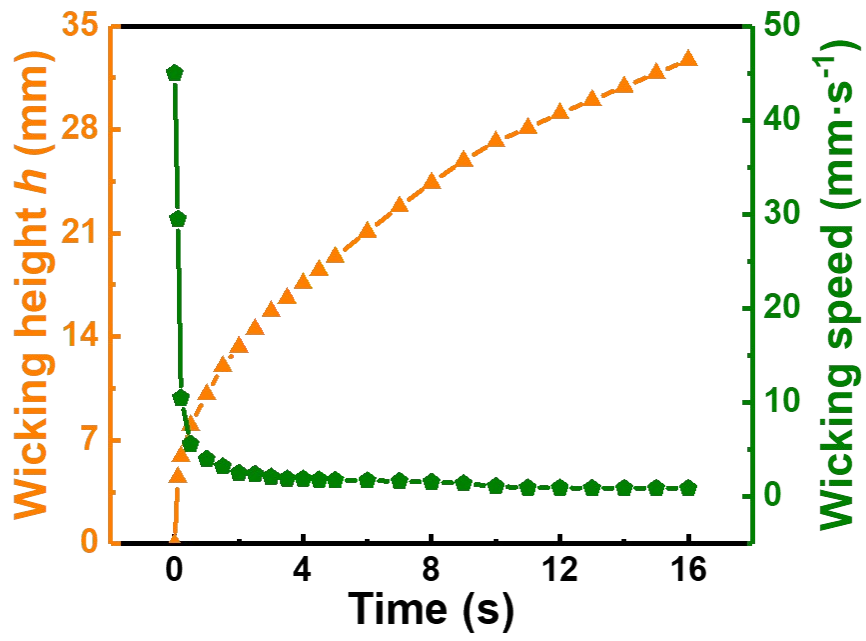


Figure S6. The wicking performance of micro-nano cones surface.

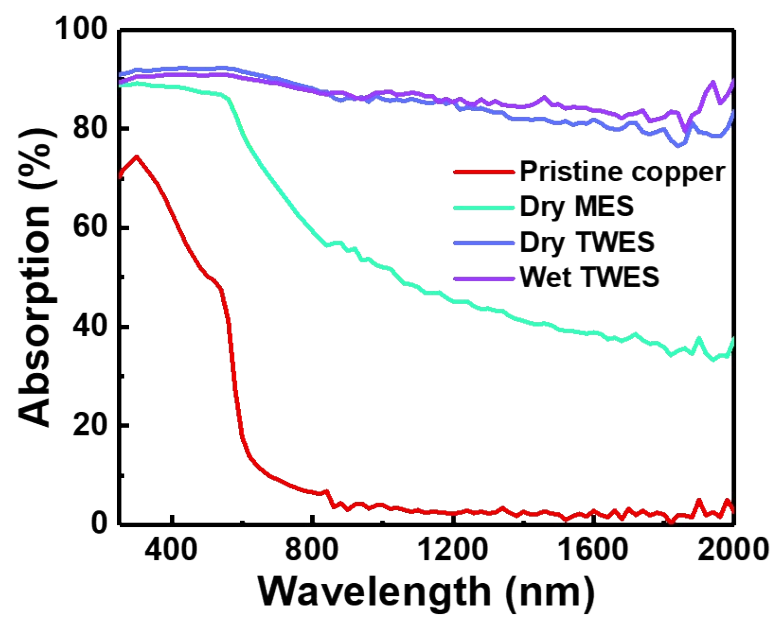


Figure S7. The absorption spectra of pristine copper, MES, dry TWES and wet TWES.

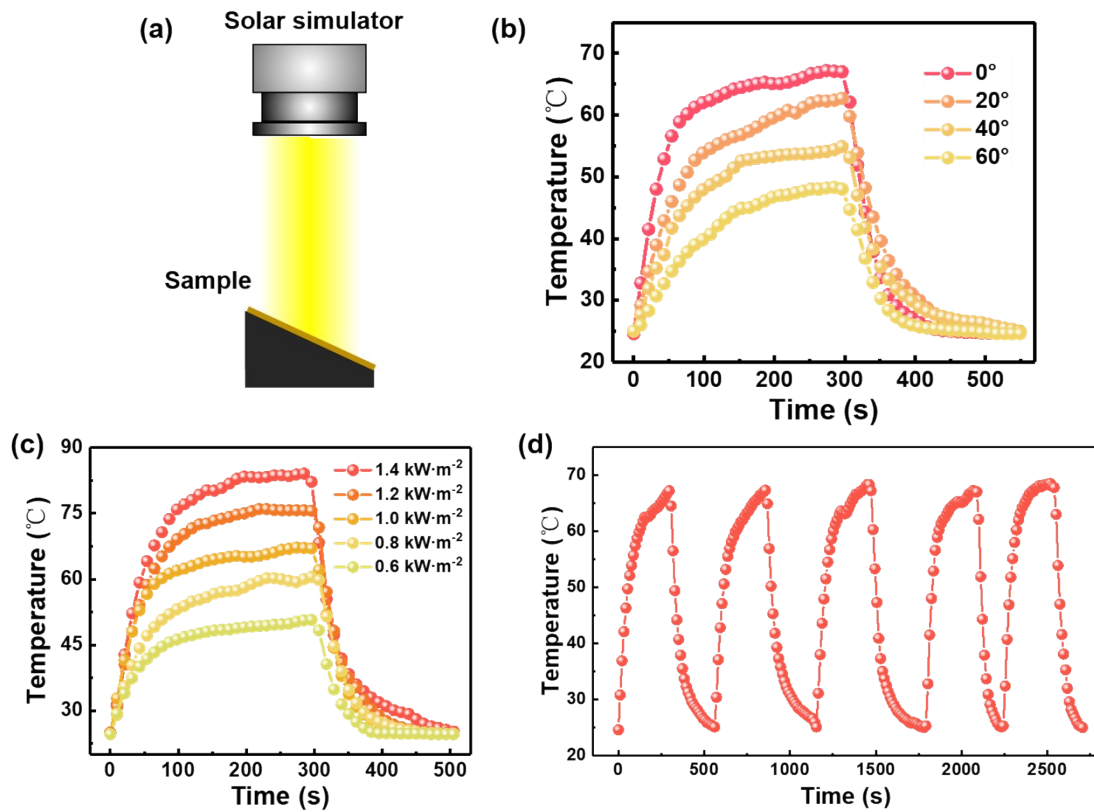


Figure S8. (a) Schematic diagram of the temperature variation experimental set-up; (b) Temperature variation over time of the TWES with different placement angles under one Sun irradiation; (c) Temperature variation over time of the TWES under different solar irradiation intensity; (d) Five temperature rising cycle of the TWES under one Sun irradiation.

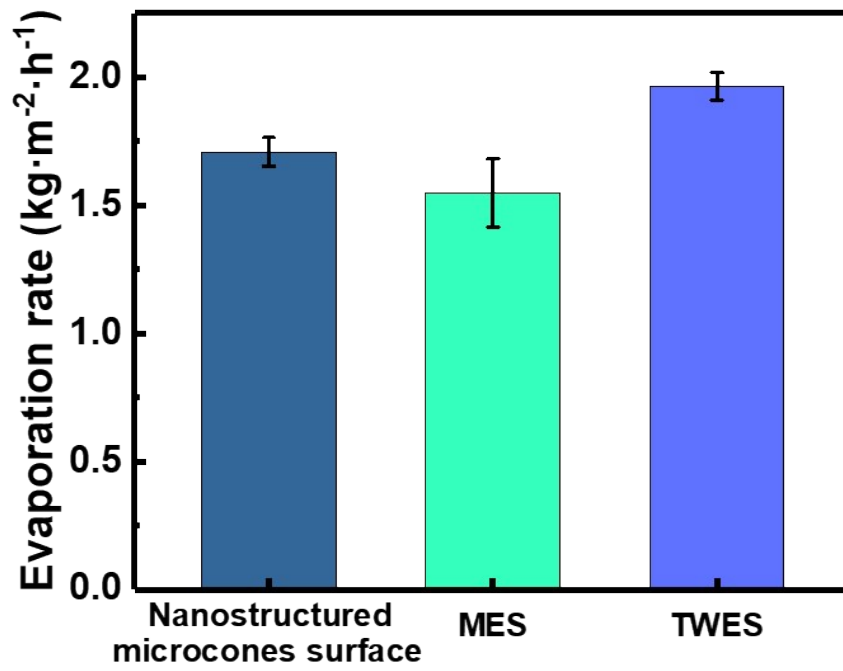


Figure S9. The evaporation rate of nanostructured microcones surface, MES, and TWES under one Sun irradiation.

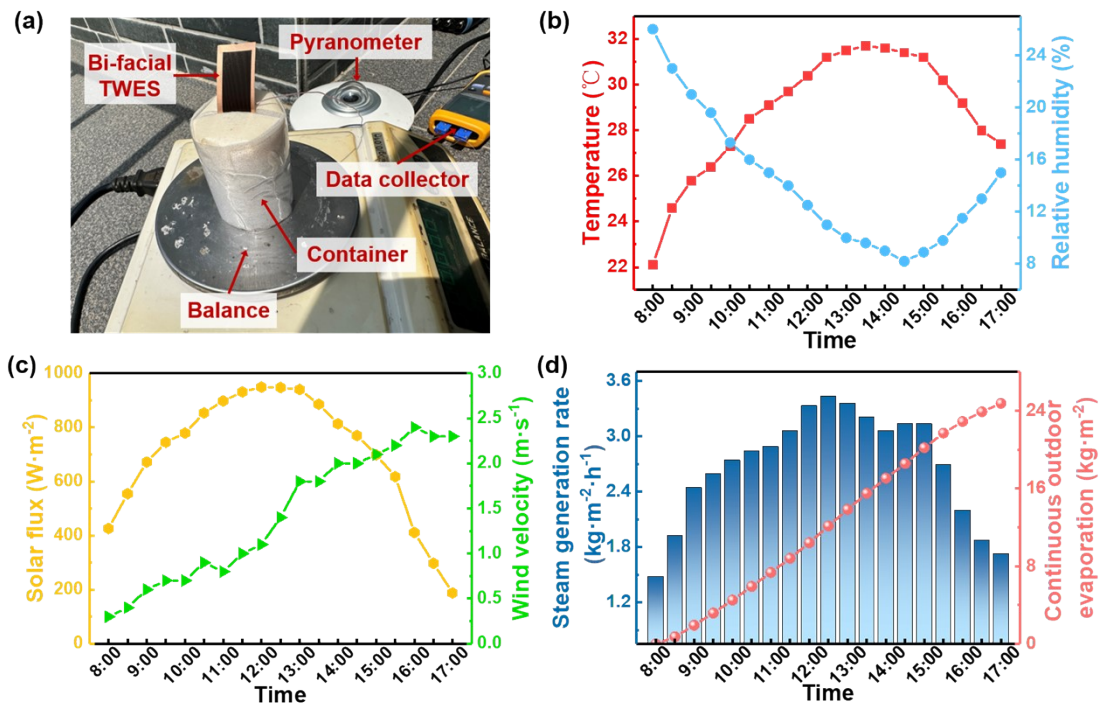


Figure S10. The outdoor solar-driven steam generation performance of the bi-facial TWES. (a) Optical photograph of outdoor experiment; Outdoor air temperature and humidity (b), solar intensity and wind velocity (c), and mass change and steam generation rate of the system (d) on a rooftop in Tsinghua University (8:00 to 17:00, May 10, 2023, Beijing, China).

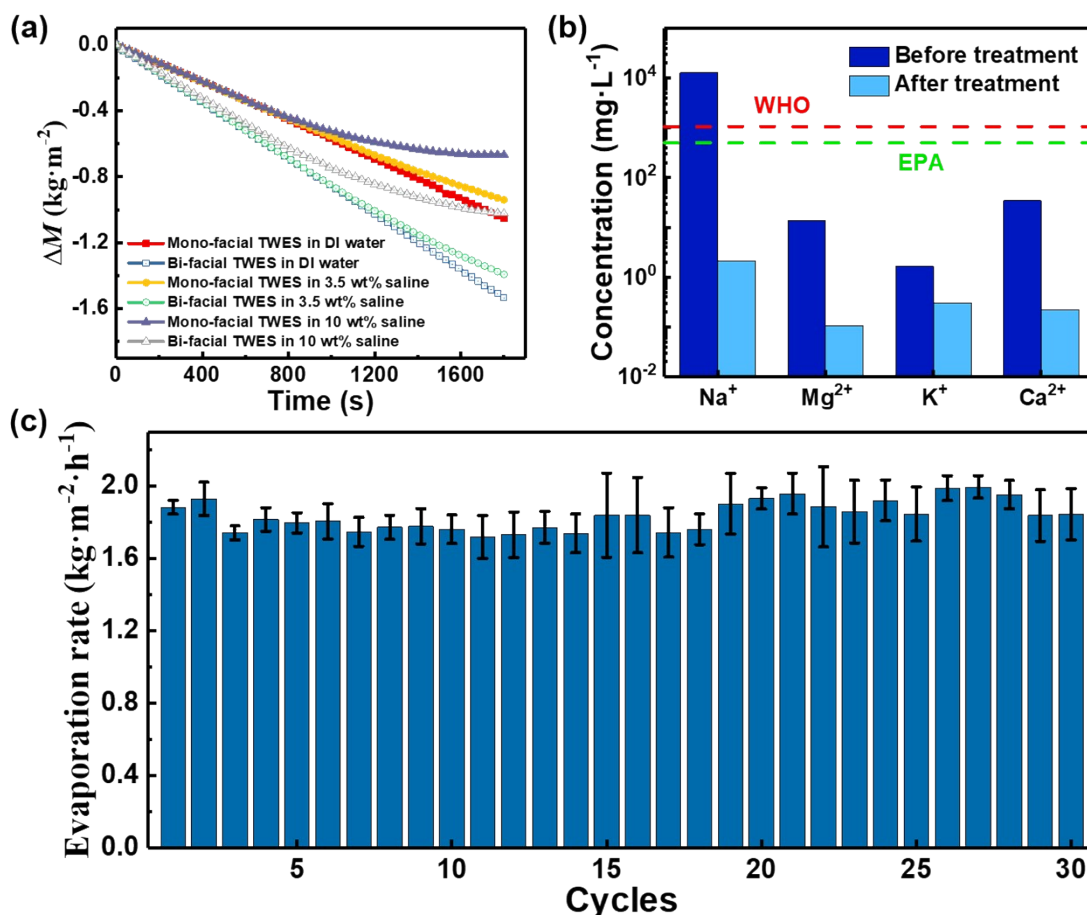


Figure S11. The evaporation performance of the TWES in saline. (a) Water mass change of TWESes in DI water, 3.5 wt% saline, and 10 wt% saline under one Sun irradiation (the evaporation performance was gradually undermined due to the salt accumulation); (b) Concentrations of four primary ions in artificial 3.5 wt% saline before and after treatment; (c) Recyclability of bi-facial TWES in 3.5 wt% saline under one Sun irradiation for 30 cycles (for each cycle, the evaporation performance of TWES was measured for 1 hour and then the sample was immersed in 3.5 wt% saline for 23 hours).

Table S1. Surface atomic ratios of the MES and the TWES.

Element	Cu	C	O	Others
MES	73.9%	15.6%	9.5%	1.0%
TWES	47.6%	31.3%	19.4%	1.7%

Table S2. The calculation of the cost for fabricating 1 m² TWES.

Items		Unit Price	Amount	Total Price
Materials	Copper	24.2 \$ m ⁻²	1.02 m ²	24.66 \$
Electricity	Nanosecond laser fabrication	0.07 \$ (kWh) ⁻¹	19.4 kWh	1.36 \$
	Femtosecond laser fabrication	0.07 \$ (kWh) ⁻¹	555.6 kWh	38.89 \$
Total		-	-	64.91 \$

References

1. Hu, H.; Sun, Y., Effect of nanostructures on heat transfer coefficient of an evaporating meniscus. *International Journal of Heat and Mass Transfer* 2016, *101*, 878-885.
2. Yu, Z.; Gu, R.; Tian, Y.; Xie, P.; Jin, B.; Cheng, S., Enhanced Interfacial Solar Evaporation through Formation of Micro - Menisci and Microdroplets to Reduce Evaporation Enthalpy. *Adv Funct Mater* 2022, *32* (17), 2108586.
3. Robbins, M. O.; Andelman, D.; Joanny, J. F., Thin liquid films on rough or heterogeneous solids. *Phys Rev A* 1991, *43* (8), 4344-4354.
4. Hu, H.; Weinberger, C. R.; Sun, Y., Effect of nanostructures on the meniscus shape and disjoining pressure of ultrathin liquid film. *Nano Lett* 2014, *14* (12), 7131-7137.
5. Lu, Q.; Shi, W.; Yang, H.; Wang, X., Nanoconfined Water-Molecule Channels for High-Yield Solar Vapor Generation under Weaker Sunlight. *Adv Mater* 2020, *32* (42), e2001544.
6. Niu, R.; Ding, Y.; Hao, L.; Ren, J.; Gong, J.; Qu, J., Plant-Mimetic Vertical-Channel Hydrogels for Synergistic Water Purification and Interfacial Water Evaporation. *ACS Appl Mater Interfaces* 2022, *14* (40), 45533-45544.
7. Zhang, S.; Wei, H.; Zhang, Z.; Zhang, J.; Bao, H.; Zhang, W., A bioinspired solar evaporator with a horizontal channel-like framework for efficient and stable high-salinity brine desalination. *Nanoscale* 2022, *14* (16), 6066-6074.
8. Wang, Y.; Hu, J.; Yu, L.; Wu, X.; Zhang, Y.; Xu, H., Recent strategies for constructing efficient interfacial solar evaporation systems. *Nano Research Energy* 2023, *2*, e9120062.